Cryogenic Thermal Fracturing of Wellbores under True Triaxial Confining Stresses - Experimental Investigation

Minsu Cha, Texas A&M University; Naif B. Alqahtani, King Abdulaziz City for Science and Technology; Bowen Yao, Xiaolong Yin, Colorado School of Mines; Timothy J. Kneafsey, Lawrence Berkeley National Laboratory; Lei Wang, Yu-Shu Wu, and Jennifer L. Miskimins, Colorado School of Mines

Abstract

A laboratory study of cryogenic fracturing was performed to test its ability to improve oil/gas recovery from low-permeability reservoirs. Our objective is to develop well-stimulation technologies using cryogenic fluids, e.g. liquid nitrogen (LN) to increase permeability in a large reservoir volume surrounding wells. The new technology has the potential to reduce formation damage caused by current stimulation methods as well as minimize or eliminate water usage.

The concept of cryogenic fracturing is that sharp thermal gradient (thermal shock) created at the surfaces of formation rocks by applying cryogenic fluid can cause strong local tensile stress and initiate fractures. We developed a laboratory system for cryogenic fracturing under true-triaxial loading, with liquid nitrogen delivery/control and measurement systems. The loading system simulates confining stresses by independently loading each axis up to about 5000 psi on 8"×8"×8" cubes. Both temperature in boreholes and block surfaces and fluid pressure in boreholes were continuously monitored. Acoustic and pressure-decay measurements were obtained before and at various stages of stimulations. Cubic blocks (8"×8"×8") of Niobrara shale, concrete, and sandstones were tested, and stress levels and anisotropies varied. Three schemes were considered: gas fracturing without cryo-stimulation, gas fracturing after low-pressure cryogen flow-through, and gas fracturing after high-pressure cryogen flow-through.

Results from pressure decay tests show that liquid nitrogen stimulation clearly increases permeability, and repeated stimulations further increase the permeability. Acoustic velocities and amplitudes decreased significantly following cryo-stimulation indicating fracture creation. In the gas fracturing without the stimulation, breakdown (complete fracturing) occurs suddenly without any initial leaking, and major fracture planes form along the plane containing principal stress and intermediate stress directions as expected theoretically. However, in the gas fracturing after cryogenic stimulations, breakdown occurred gradually and with massive leaking due to thermal fractures created during stimulation. In addition, the major fracture direction does not necessarily follow the plane containing principal stress direction, especially at low confining stress levels. In tests, we observed that cryogenic stimulation seems to disrupt the internal stress field. The increase in borehole temperature after stimulation affects the permeability of the specimen. When a stimulated specimen is still cold, it maintains high permeability because fractures remain open and local thermal tension is maintained near the borehole. When the rock warms back, fractures close and permeability decreases. In these tests, we have not used proppants. Overall, fractures are clearly generated by low and high-pressure thermal shocks. The added pressure of the

high-pressure thermal shocks helps to further propagate cryogenic fractures generated by thermal shock. Breakdown pressure is significantly lowered by LN stimulation with breakdown pressure reductions up to about 40% observed.

Introduction

To improve well productivity and hydrocarbon recovery in unconventional plays, almost all horizontal or vertical oil and gas wells are completed with some kind of stimulation. Massive hydraulic fracturing using water-based fluids has been demonstrated as one of the most effective technologies that is widely applied in conjunction with horizontal drilling for developing shale and tight reservoirs (Steward 2013). The commonly used slickwater is prepared by mixing proppants and a minute amount of chemical additives into water, which is readily available and of low cost (Sharma et al. 2004, Shaefer 2005).

Massive hydraulic fracturing using water-based fracturing fluids poses several major challenges. First, water can severely damage the clay-rich shale formations in the sense that clay minerals are apt to absorb water and swell, thus narrowing the conductive fractures and effective pores. Also, capillary retention of water in tiny pores would partially or completely block the flow path of hydrocarbon from the matrix to fracture networks, impairing the relative permeability of hydrocarbons (Mazza 1997, Wang et al. 2016). Secondly, large quantities of water used in massive fracturing are concerning, placing demands upon local water supply and environments, especially in arid areas with water shortages. Statistics show that during 2009-6/2011, the median water usage in hydraulic fracturing in Texas for each horizontal well in Barnett, Eagle Ford, and Haynesville were 10,600, 16,100, and 21,500 m^3, respectively (Nicot and Scanlon 2012). The lower volume of 10,600 m^3 can fill more than two Olympic swimming pools or supply water for 65 families for one year. Finally, high-pressure injection of fracturing fluids containing chemical additives has caused a contentious community and political climate over groundwater contamination. Different from hydraulic fracturing, cryogenic fracturing using liquid nitrogen (LN) offers potentially greater fracturing capabilities without any of these water-related issues.

Cryogenic fracturing is a relatively new technology for unconventional reservoir stimulation that is meant to expand and supplement the traditional hydraulic fracturing operations. Cryogenic fracturing exerts a sharp thermal gradient created by contacting a cryogen to a much warmer rock under reservoir conditions to induce fractures. Cryogen takes a liquid form at low temperatures and transforms into the gaseous phase at standard conditions, such as LN and liquid carbon dioxide. Specifically, when LN is injected into a borehole, heat from the rock near the borehole will quickly boil the liquid nitrogen (LN boiling point at atmospheric pressure is -195.8ºC or -320.4ºF), resulting in rapid cooling and contraction of the near-borehole reservoir rock. Once the contractive tension increases to sufficiently high level, fractures orthogonal to the rock surface can be initiated (Cha, Alqahtani, Yao, Wang, et al. 2016). These newly induced fractures can be further extended by high-pressure gas generated from LN vaporization. Note that nitrogen has a liquid-to-gas expansion ratio of 1:694 at room temperature (20°C or 68°F) and atmospheric pressure.

Although during the shale boom cryogenic fracturing has not been widely deployed, it was tested in a few field pilot tests in the 1980s and 1990s. To improve the recovery of low-permeability sandstone reservoirs, Lillies and King

(Lillies and King 1982, King 1983) pumped gelled liquid carbon dioxide at -28.9ºC to -40ºC (-20 ºF to -40ºF) to stimulate wells with standard tubing and casing configurations. The liquid CO_2 system does not damage formations and reverts to the gaseous state under reservoir temperature. In general, oil and gas wells were cleaned up within 3-4 days after the fracturing injections. Due to higher viscosity than pure liquid CO_2, gelled CO_2 was capable of carrying sand proppants to prop the induced fractures open. All the wells that were stimulated with gelled CO_2 showed positive responses in production rates (Lillies and King 1982, King 1983).

In early laboratory studies of LN fracturing, McDaniel et al. (1997) immersed coal samples in LN to observe the cryogenic fracturing process. The coal samples significantly shrank and broke into smaller cubic fragments as a result of generated or activated microfractures (cleats) orthogonal to the coal surface. It was also found that repeated exposure cycles to LN further broke the coal samples into even smaller pieces. After three cycles of LN submersion and warm-up to ambient temperature, the coal sample tested was reduced to grain-size particles. McDaniel et al. (1997) then continued fracturing treatment with liquid nitrogen in field tests and reported production rates for five wells before and after the stimulation operations. The results showed that three coalbed methane wells experienced increased production, one coalbed methane well showed unchanged production, and one low permeability sandstone well initially completed with slickwater fracturing decreased in production rate. Grundmann et al. (1998) later treated a Devonian shale well with LN and observed an incremental production rate of 8% compared to a nearby offset well that was fractured with nitrogen gas. The increased production rate in this field test suggests the efficacy of cryogenic fracturing using LN, but there could be several reasons for an offset well in a shale formation that might produce at a lower rate, including anisotropic in-situ stresses and heterogeneous formation conditions.

LN and liquid carbon dioxide have low viscosities (Rudenko and Schubnikow 1968, Fenghour et al. 1998), and therefore they cannot carry conventional high-density proppants normally carried by viscous fluids. Gupta and Bobier (1998) suggested that it is possible to increase the injection rate of liquid CO_2 to improve proppant transport efficiency, though normally it is incapable of transporting adequate proppant. The turbulence caused by high flow rate allows sufficient suspension of common proppant, at least from the wellbore into the perforation clusters, if not through the outreaching fractures (Gupta and Bobier 1998). Some studies even showed that cryogenic fracturing might rely less on proppant compared to conventional hydraulic fracturing. The experiments of McDaniel et al. (1997) demonstrated that coal rubblization after cryogen contact could act as a self-propping mechanism. That is to say, if the fracture plane rock experiences sufficient thermal-induced breakage, then the rubblized particles may prop the fracture open against in-situ stresses during the warm up and closure of the cryogenic fractures. Even if neither conventional proppants nor self-propping mechanisms can effectively take place, ultra-light weight proppants (ULWPs) may be a good candidate to be tested. ULWPs are chemically synthesized proppants consisting of a hardened core with multiple layers of outer resin coating (Kendrick et al. 2005). With ULWPs, Kendrick et al. (2005) obtained improved post-treatment production rates from wells stimulated by nitrogen foam in Devonian shale. In comparison with those treated with traditional proppants, the majority of the wells treated with ULWPs performed as well or even better.

During the past two decades, no further studies have been conducted to better understand and apply cryogenic fracturing technology. The fracturing mechanisms and major factors controlling cryogenic fracturing processes are poorly understood. With the increasing development of unconventional reservoirs and the rising cost of acquiring water in some plays, it is necessary to carry out research to further investigate this water free and hence formation damage free and environment-friendly fracturing technology and to discover the significant potentials it can provide for the oil and gas industry. This study aims to better understand and optimize the cryogenic fracturing processes using liquid nitrogen and discusses how it can be integrated into our current fracturing technology to enhance the oil and gas recovery from unconventional oil and gas reservoirs.

Simple preliminary cryogenic tests were conducted to understand the LN and material behaviors by performing submersion tests and applying LN to boreholes in unconfined concrete specimens (Cha et al. 2014). Data gathered from the previous study provided a basic understanding of physical mechanisms. In this study, we investigated the effect of cryogenic stimulation on rock fracturing under true triaxial confining stresses. We developed laboratory setups and procedures that are designed for conducting cryogenic fracturing tests under wellbore conditions. In these tests, LN was flowed through boreholes drilled in rock blocks including concrete, shale, and sandstone under triaxial confining stresses. Fracturing processes were thoroughly monitored to observe the behaviors associated with cryogenic treatment. Fracture development was assessed by acoustic measurements, permeability measurements, and visual inspection. Comparisons were made between pre- and post-stimulation conditions to evaluate the efficiency of this technique. The results will help to select efficient applications of cryogenic stimulations as a stimulation technique and will set the foundations for continuing avenues of research.

Laboratory Studies

The devices and procedures used in our tests are significantly optimized and improved based on understanding cryogen and fluid behavior from our preliminary studies. Artificial and natural rock specimens were prepared for the experiments. Shale and sandstones were obtained from outcrops of oil and gas producing formations.

Experimental Equipment

A laboratory system for cryogenic stimulation study under true-triaxial loading conditions has been developed. It consists mainly of a triaxial loading device, an LN delivery, and control/measurement system (Figures 1 and 2). More details of the laboratory system are reported in Cha et al. (2017).

Triaxial loading system

The true-triaxial loading system was developed to simulate the effects of stress levels and anisotropies manifested *in situ* on the characteristics of cryogenic fracturing. The containment was designed for the selected specimen size 8"×8"×8". The true-triaxial loading (TX) system can load the specimen up to 4500 psi along the x- and y-axes, and 6000 psi along the z-axis, and we can independently control loadings on the three axes. Three pneumatic pumps power

the two hydraulic actuators (x-and y-axes) and the hydraulic press (z-axis). One advantage of the system is the vertical load frame can be moved by rolling sideways on the bed. This provides space to work on specimens inside the containment. An open system (outer surface of the specimen under stress but not under fluid pressure) is preferred in our study to better manage unexpected conditions such as a cryogen spill, and for application of instrumentation (Figure 1).

PTFE or silicon pads were placed between specimens and the loading platens to provide as uniform contact and loading as possible to specimen surfaces. PTFE or silicon pads resist temperature down to −350°F and −80°F, respectively. A servo control system for automatic load control is not available on our device, nor required as the loadings are quasi-static. Constant forces were achieved by manual control or in a quasi-automatic manner using pressure relief valves attached to the hydraulic lines. In the manual control tests, when a certain amount of pressure decay occurs in the hydraulic system, a small amount of pressure is added by pumping accordingly.

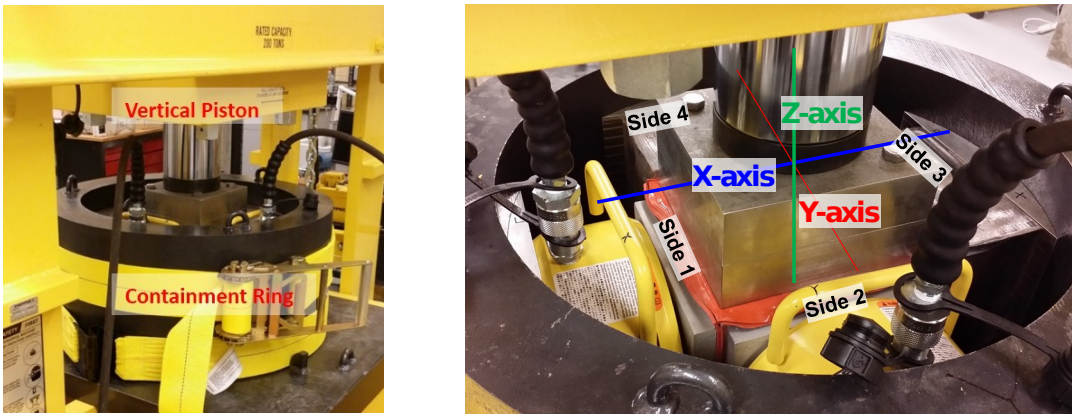

(a) **(b)**

Figure 1—True triaxial loading device: (a) Containment ring housing the specimen and actuators, (b) Closeup inside the ring showing the axes and the faces of the specimen.

Liquid nitrogen delivery

The cryogen flows from the dewar once an outlet valve is opened by the nitrogen gas pressure generated inside the dewar (Figure 2). This pressure was usually maintained at low levels about 10-20 psi. The fluid injection/delivery system for cryogenic stimulations needs to be fundamentally different from that for hydraulic fracturing. For cryogenic thermal fracturing, cryogen needs to flow through and be replenished in order to decrease the temperature of boreholes, because liquid nitrogen will rapidly vaporize obtaining its heat of vaporization from the much hotter rock. Compressed nitrogen gas was used to push liquid nitrogen into boreholes under higher pressure (“higher-pressure LN flow”) and pressurize boreholes to perform the breakdown test. Pressure can be applied as shown on the right-hand side of Figure 2.

Tubing and fittings in the cryogen transport lines must withstand cryogenic temperature (down to −321°F in our study). We used stainless steel 316 and brass for cryogen transport, which provide such an ability as their brittleness-ductility transition temperature is lower than liquid nitrogen boiling point. Stainless steel has a higher pressure rating at the cryogenic temperature than brass. Tubing for

higher-pressure applications at the cryogenic temperature must be seamless and annealed. 1-inch stainless steel tubing was used for borehole casing in our tests and is affixed to the borehole wall by epoxy for sealing and pressure resilience. Epoxy generally worked well for that purpose but could deteriorate after 3-5 cycles of LN exposure. Insulation was applied to the lines between Dewar and specimen inlet to minimize heat transfer.

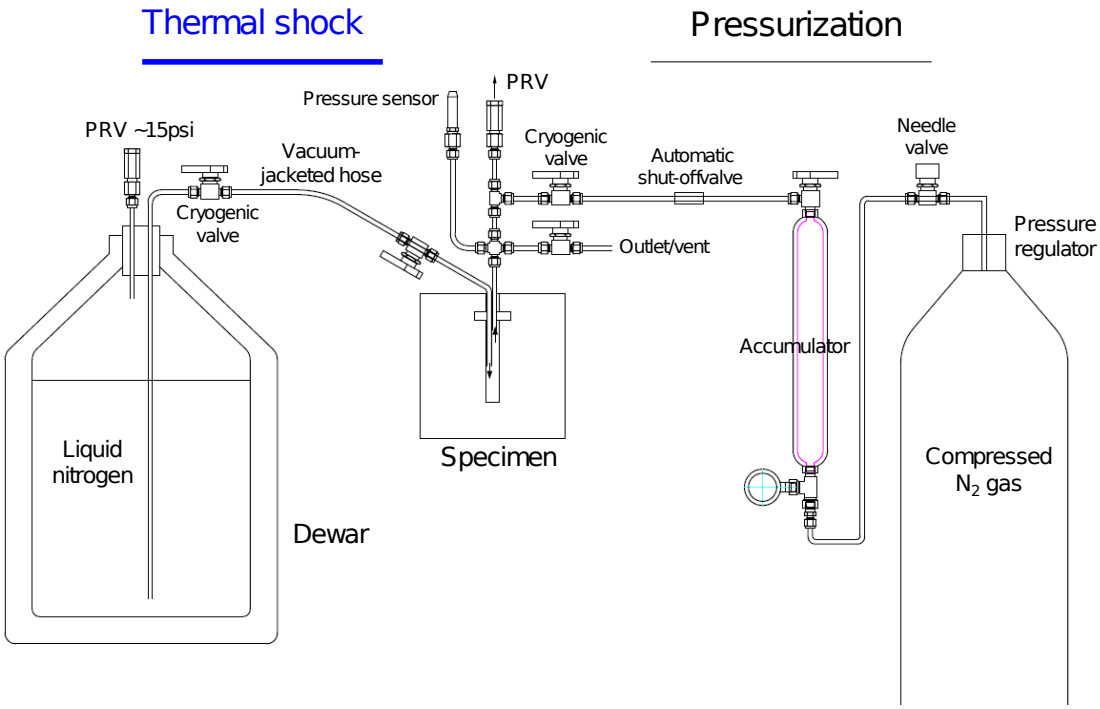

Figure 2—Cryogenic fracturing schematic (true triaxial loading system not shown).

Measurements & monitoring

Measured parameters include pressure, temperature, liquid nitrogen consumption, and photos of specimen surfaces. The pressure was recorded through a pressure sensor placed at the end of a stand-off tube (Figure 2), where a vapor cushion hinders conductance of the cold temperature to the sensor. Data show that the temperature at the tip of the stand-off tube is well above 0°C throughout the stimulation (Figure 3). The tube is not to be longer than necessary as a long narrow tube create drag and thus decrease responsiveness to rapidly-changing pressure. For temperature measurement, T-type thermocouples were chosen for accuracy and range. Very thin thermocouple wires were inserted into borehole between casing and borehole walls. One thermocouple is hanging in the borehole to measure temperature in the borehole, and another is attached to the borehole wall to observe the temperature of the wall. Liquid nitrogen consumption was measured by putting the Dewar on a balance. In addition, acoustic waves were utilized for assessments of fractures before and after treatments.

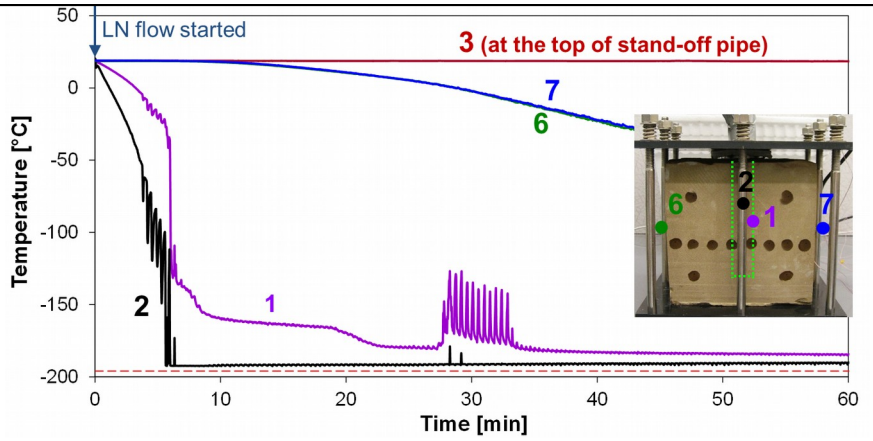

Figure 3—Temperature data from five thermocouples during a low-pressure LN borehole flow-through for an unconfined specimen - locations of thermocouples are shown in the inset.

Test procedures

Cryogenic stimulations are accomplished by applying liquid nitrogen to the borehole in a specimen. Baseline conditions of a specimen relevant to fracture indications were measured before treatments, and then the same measurements were performed during treatments or after completing the treatments to allow comparisons. Assessments of fractures include acoustic waves, pressure decay, and visual observations.

Stimulation procedures

As stated earlier, boiling LN is needed to lower temperature and the cryogen needs to be continuously flowed through the borehole. Using the cryogenic fracturing apparatus under true-triaxial loading, we performed two cryogenic stimulation schemes: 1) low-pressure liquid nitrogen flow and 2) high-pressure liquid nitrogen flow. In the low-pressure liquid nitrogen flow scheme, liquid nitrogen was flowed from the dewar due to a pressure difference between the inside and the outside of the dewar upon opening the dewar outlet valve. Pressure ranged from 5 to 20 psi in the borehole, depending on the internal pressure of the dewar. In the high-pressure scheme, liquid nitrogen was flowed through the borehole under higher pressure (300-400 psi) for quicker cooling in the borehole due to increased gas density and reduced film boiling effects. In the high-pressure flow scheme, the higher borehole pressure may facilitate fracture opening by helping to reach tensile strengths of specimens. Typically, higher-pressure stimulations were applied multiple times because our vessel for storing liquid nitrogen for higher-pressure injection is small (1 liter), which makes each stimulation cycle very brief (1-2 min). Nitrogen, which was liquid before entering the borehole, initially exits the borehole as gas and later as a gas/liquid mixture as the borehole cools. Gas/liquid leaving the borehole was not recovered in either stimulation schemes.

Assessments of fractures

Assessments of fractures were made by borehole pressure decay tests, acoustic measurements, and breakdown pressures (P_{BD}). Borehole pressure decay tests were performed by applying pressure to the borehole, shutting the borehole in,

and monitoring the pressure decay. This was done before cryogenic treatments, between treatments, and after completing the cryogenic treatments. After all planned stimulations were completed for a specimen, the specimen was subject to a high gaseous nitrogen (GN) pressure to fully fracture ("breakdown") the block. The P_{BD} of different treating schemes were compared with the baseline P_{BD} of the non-LN-treated specimen. Breakdown tests were performed last, as they fully fracture the specimens.

Transmission of compressional (p-waves) and shear (s-) acoustic waves were recorded before and after the treatments. Post-stimulation measurements were performed before applying the final P_{BD}, so that we can quantify the effect of cryogenic stimulations. The characteristics of acoustic waves propagating through the medium depend on the mechanical properties of the medium. In particular, the wave velocity in jointed rock masses is a function of the density of fractures (or fracture spacing) (Cha et al. 2009). When other properties such as intact rock properties, density, and joint stiffness are the same, the wave velocity can be used as a monitoring tool to characterize fracture generation.

Specimens

Collection and preparation

Shale and sandstone were collected from outcrops of oil and gas producing formations to make specimen types more relevant to the purpose of this study. Specifically, we used Niobrara shale blocks gathered from an outcrop of the Niobrara formation in Lyons, Colorado, and sandstone blocks gathered from an outcrop of Williams Fork Formation in Western Colorado. A fairly large specimen size (8"×8"×8") was selected for the study so that sufficient thermal gradients could be created inside the specimen for an extended time, which may be required for thermal tensile fracturing. They were precisely cut into the desired size using a bridge saw (Cha, Alqahtani, Yao, Yin, et al. 2016).

Concrete specimens made of cement and sand were used as surrogates for rocks. A fresh concrete with a water to cement ratio of 0.55, and sand to cement ratio of 2.5 was mixed and poured into a 8" cubic mold and sealed in a plastic bag. After 24 hours, the seal and mold were removed, and the concrete block was cured under water (ASTM 2014a) for at least two months, which maximizes hydration enhancing concrete strength.

Prior to cryogen stimulations, a 1-inch diameter borehole was drilled into prepared 8"×8"×8" specimens using a diamond coring drill bit with 1.06-inch diameter under dry conditions and the borehole was drilled to a depth of six inches. A 1-inch stainless steel-316 casing was then attached to the borehole with epoxy after the thermocouples were inserted into the borehole. The casing extends two inches into the borehole.

Intact rock properties

Basic index properties of intact specimens are listed in Table 1. Key intact rock properties were obtained and may allow more quantitative approaches to further analyze results. Mechanical, thermal, and flow properties of the specimens were tested and obtained. Porosity and permeability were measured using a CMS 300 automated permeameter (CoreLab). Dynamic elastic constants were calculated from densities and acoustic wave velocities (Cha and Cho 2007). Static Young's

modulus, unconfined uniaxial compressive strength, and splitting tensile strength were measured according to the ASTM standards (ASTM 2008, 2014b). Specific heat capacities were measured using a calorimeter, and linear thermal expansion coefficients were measured using core specimens.

Table 1—Mechanical, thermal, and flow properties used for cryogenic fracturing test under confinement.

Properties \ Rock Type	Concrete	Sandstone	Shale
Density (g/cm^3)	2.04	2.18	2.39
Unconfined compressive strength (MPa)	37.3	41.5	54.6
Splitting tensile strength (MPa)	2.88	4.51	8.45
Static Young's Modulus (GPa)	26.2	-	41.6
Dynamic Young's Modulus (GPa)	30.6	44.9	47.5
Dynamic shear Modulus (GPa)	12.3	18.4	18.7
Poisson's ratio	0.24	0.22	0.27
P-wave velocity (m/s)	4220	4850	4970
S-wave velocity (m/s)	2455	2906	2796
Specific heat capacity (J/(kg·K))	891	857	990
Linear thermal expansion coefficient (K^{-1})	1.3×10^{-5}	-	1.1×10^{-5}
Porosity (%)	9.56	11.5	6.64
Permeability (md)	8.72×10^{-3}	0.349	1.06×10^{-3}

Results and analyses

Eight concrete specimens, four shale specimens, and two sandstone specimens were tested under different triaxial confining stresses and with different cryogen treatment procedures as shown in Table 2. The results are analyzed, compared and discussed here. In what follows, we will first present measurements of temperature and pressure in boreholes during treatments and subsequent breakdown tests, and then present the effects of cryogenic stimulations on fracture patterns, permeability changes, and acoustic data.

Temperature and pressure in boreholes

Breakdown tests were first performed on untreated specimens #16 and #17. In these tests, GN was used to pressurize the borehole and fracture the specimens (Figure 4). The breakdown pressures (P_{BD}) were recorded as the baseline P_{BD} to be compared with those for specimens stimulated with LN. Breakdown by gas pressure on untreated specimens is characterized by a sudden loud fracture without any pre-leaking of gas. Indications of specimen fracture were also noted from the pressure response in the hydraulic lines connected to the loading actuators. As exemplified in Figure 4b, the x-axis hydraulic line responded to the breakdown with a high jump in the hydraulic pressure. This brief jump in the x direction is due to the sudden opening of the fracture in the minimum horizontal stress direction (x-axis) (fractures propagated along a plane perpendicular to the minimum horizontal stress direction), as confirmed later by visual inspection of the fractures. Fracture initiation and propagation was so sudden that the loader did not have enough time to maintain constant load.

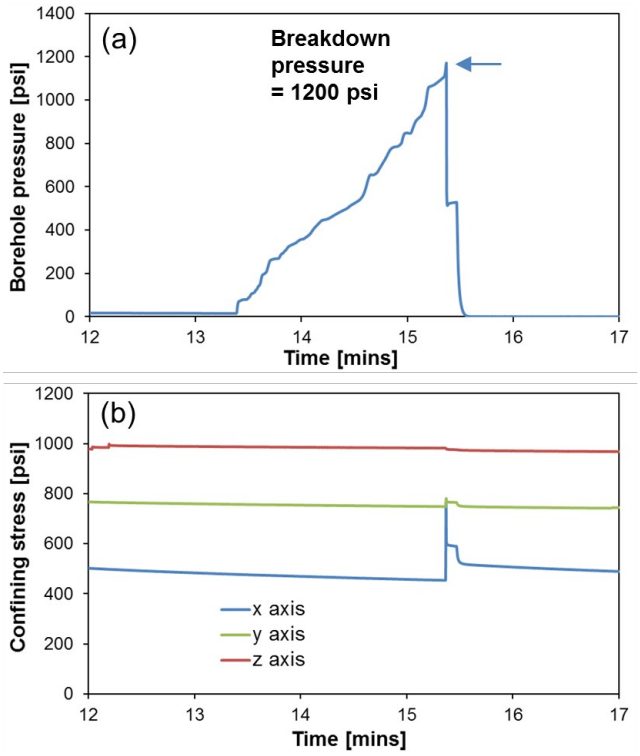

Figure 4—Breakdown fracturing test (using gas pressure) of a specimen without LN treatment (Specimen #17).

Figures 5 and 6 present typical temperature and pressure evolutions during low-pressure liquid nitrogen flow and high-pressure liquid nitrogen flow through boreholes. For low-pressure injection, the temperature dropped quickly; however, on the borehole wall, the rate of temperature drop is retarded compared to that of the borehole (Figure 5a) due to the Leidenfrost effects (film boiling). Cryogen pressure in the borehole remained low (10-15psi) (Figure 5b). For high-pressure injection, the temperature dropped more quickly than for the low-pressure treatment due to reduced effect of surface film boiling under higher pressure flow-through (Figure 6a – red curve initially overlies blue curve). The cryogen pressure during the flow-through was 250-450psi, but very brief, e.g., 1-2 min (Figure 6b). For high-pressure treatment, multiple cycles of LN treatment were performed because of the small volume of the LN container (1 liter) and thus small amount of LN available for each treatment. Upon ceasing the LN supply, the temperature in the borehole increased quickly back after these durations of stimulations.

Although probably a test artifact, the temperature reduction in borehole wall was slower in the unconfined specimen tests than the confined specimen tests (Compare Figure 3 with Figure 5). This could be due to contraction of borehole wall circumference when subjected to high confining stresses; the thermocouple, which was attached to the wall prior to the application of stresses, may have been loosened and the quality of adhesion may have been compromised by the contraction and thereby the thermocouple experienced more rapid cooling.

In gas nitrogen fracturing of untreated specimens, no pre-leaking of gas was noticed prior to breakdown. For cryogenically treated specimens, however, prior to

reaching the breakdown points, very noticeable high-pitch hissing sounds that increased with increasing borehole pressurization were heard, indicating leakage and potentially also the progression of fractures.

We performed tests that showed cryogen leaking during cryogenic stimulation, which means local break-through by cryogenic stimulation only. This occurred in both low and high-pressure injections; the approximate times for major leaking to appear are indicated by the dotted arrows in Figure 5b and Figure 6b. In higher-pressure LN flow, leaking of *liquid* nitrogen was noted during the third high-pressure LN stimulation, indicating that fractures created were significant and they have extended to the surface at least locally.

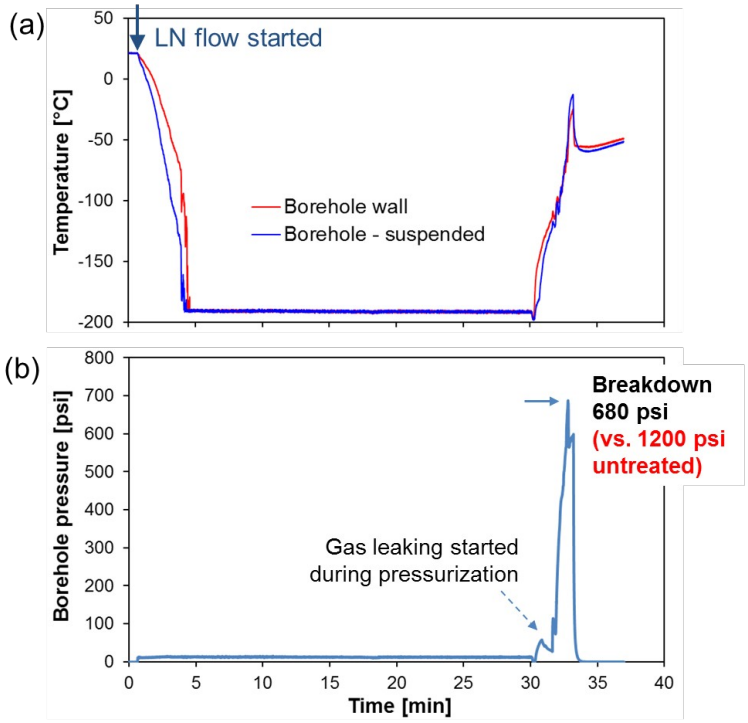

Figure 5—Temperature and pressure during low-pressure LN flow-through (Specimen #18).

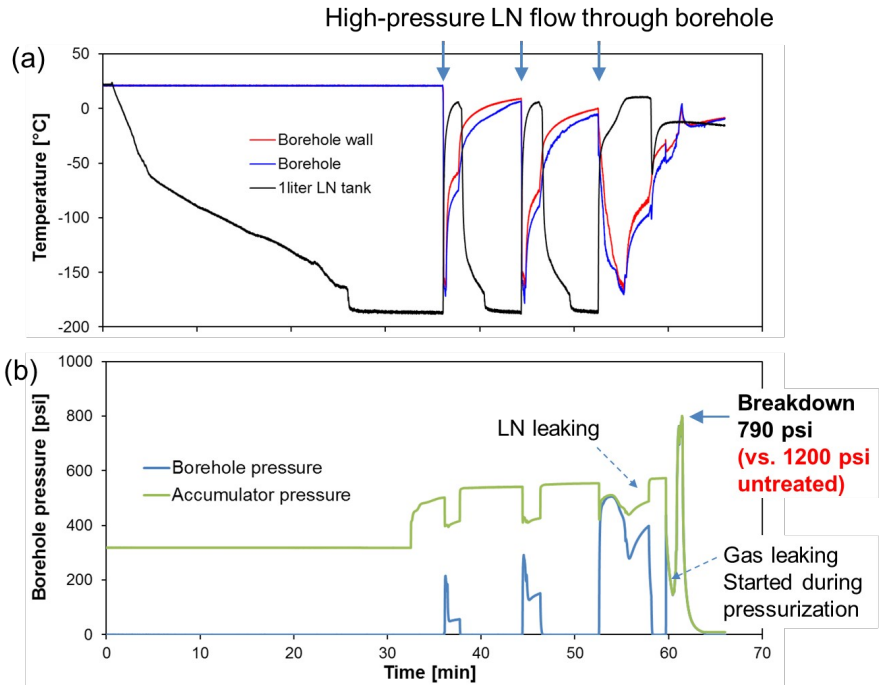

Figure 6—Temperature and pressure during higher-pressure LN flow-through (Specimen #19).

Figure 7 summarizes and compares breakdown pressures (P_{BD}) of tested shale and concrete specimens. This clearly indicates that cryogenic treatment decreases the magnitude of P_{BD} in concrete and shale specimens by both low- and high-pressure liquid nitrogen flow-through. P_{BD} reductions observed are 37% for the concrete specimens and 43% for the shale specimens. Bedding/existing cracks can lead to significantly lower P_{BD} with or without treatment.

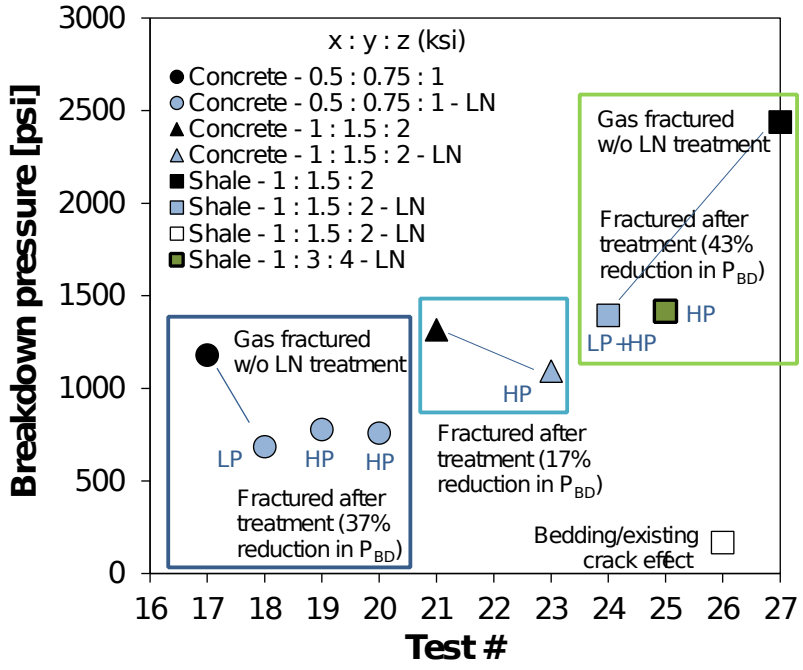

Figure 7—Effect of cryogenic stimulation on breakdown pressure levels for different rocks and stimulation conditions. LP and HP denote low- and high-pressure LN flow. See Table 2 for details.

In the breakdown tests, the gas pressure was applied to the borehole until breakdown. Due to the use of gas and the volume in the tubing and borehole, injection system compliance is large (Lecampion et al. 2016). In the case of untreated specimens, the energy stored in the compressed gas may make the pressure level of fracture initiation similar to the breakdown pressure, and breakdown immediately follows the fracture initiation (Lhomme et al. 2005, Detournay and Carbonell 1997). Indeed, we observed sudden and loud sound for all untreated specimens with sudden drop in borehole pressure. In cryogenically treated specimens, thermally induced fractures already exist near the borehole. Upon applying pressure to approach the breakdown, we observed audible gas leakage that increases with increasing pressure. When pressure reached the level needed to propagate the thermally induced fractures, breakdown took place. These breakdown pressures for the treated specimens are lower than those of the untreated specimens.

Fracture patterns

Cryogenic stimulations alone generally did not lead to fracture propagation to the surface of the specimens. Only in some long-duration stimulations, fractures propagated to the external surface. These were identified visually and/or by localized leakage of nitrogen during stimulation. Most fractures reached the surface because of the breakdown of the specimens. In this section, we present fracture patterns visible on the external surfaces of specimens after breakdown.

Untreated specimen - Direction of breakdown fractures

Breakdown fracturing of untreated specimens tended to be sudden without any pre-leaking. The major fracture direction in the untreated specimens was perpendicular to the minimum horizontal stresses direction (i.e., x-axis) from the borehole wall (Figure 8). In other words, major fracture planes tended to exist along the y-z plane, which is the plane containing the maximum principal stress direction and the intermediate stress direction. This behavior is expected from rock mechanics and also observed in hydraulic fracturing. The top view picture taken from inside the wellbore after breakdown also shows the fractures propagating perpendicular to the minimum horizontal stresses direction from the borehole wall (the upper subset photo in Figure 8a).

Effect of cryogenic stimulations on direction of fractures

We observed that if specimens are cryogenically stimulated, the breakdown fracture direction could deviate from the conventionally predicted directions. This is particularly true when the confining stress is low. For example, fractures were in rather arbitrary directions (Figure 9a&b), or occurred only locally (Figure 9c&d). The triaxial stress ratios of these blocks was x:y:z=500:750:1000psi for Figure 9a&b and x:y:z=1000:1500:2000psi for Figure 9c&d. In Figure 9b, the fracture opened in a half wing configuration along the minimum horizontal stress direction. Another fracture wing was along the maximum horizontal stress direction. In Figure 9d, the main fracture propagation was around the wellbore, affected by casing’s

much higher thermal conductivity, creating weakness in that region. These fractures occurred gradually without clear fracturing sounds and with massive pre-leaking. Clearly, cryogenic stimulation disrupts the internal stress field.

However, with larger stress anisotropy (and perhaps larger stress magnitude relative to a thermal treatment applied) in triaxial confining stresses, fractures did follow theoretically predicted directions; the fractures propagated as expected, in a plane perpendicular to the minimum horizontal stress (x-direction). At even larger stress anisotropy, we surmise that confining stress would again govern the fracture direction (e.g., Figure 10; triaxial stress x:y:z= 1000:3000:4000 psi). A comparable behavior in hydraulic fracturing in a medium with natural fractures may be that when the horizontal stress difference increases, the fracture is smoother and straighter (Beugelsdijk et al. 2000, Guo et al. 2014).

Deviation from the directions expected from stress principles may lead to more fracture tortuosity or complexity than pressure-based fracturing as observed in Figure 9 & 10, and also in Cha, Alqahtani, Yao, Wang, et al. (2016). This tortuosity or complexity may affect the fluid flow path, self propping, and the efficiency of stimulations. On the other hand, as shown in Cha, Alqahtani, Yao, Wang, et al. (2016), fully developed thermal fractures in a wellbore extend both longitudinally and radially away from the wellbore, and with tortuosity tendency, they form a rather complex network.

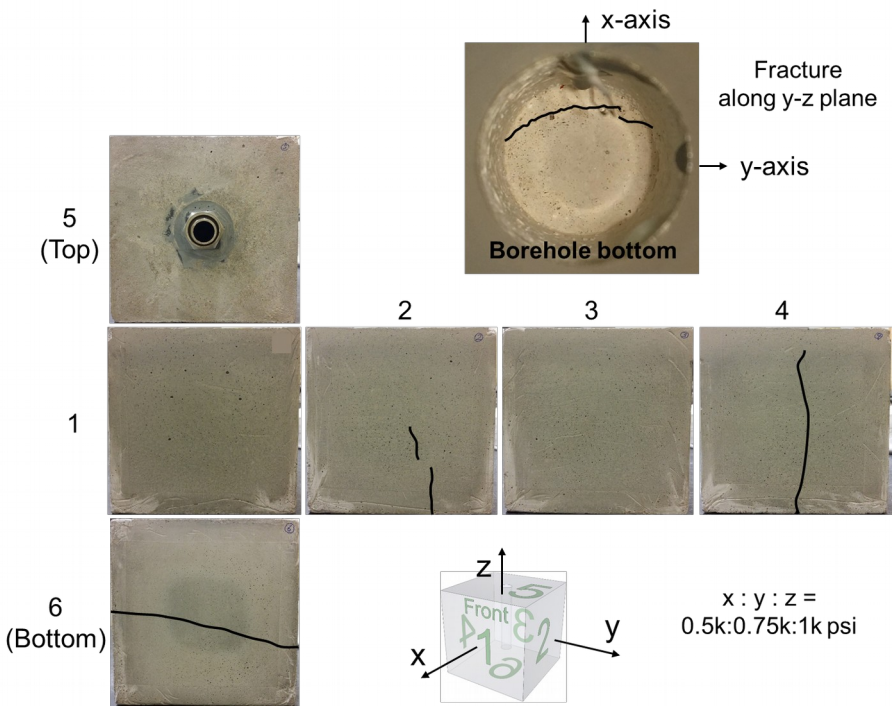

(a) Specimen #17

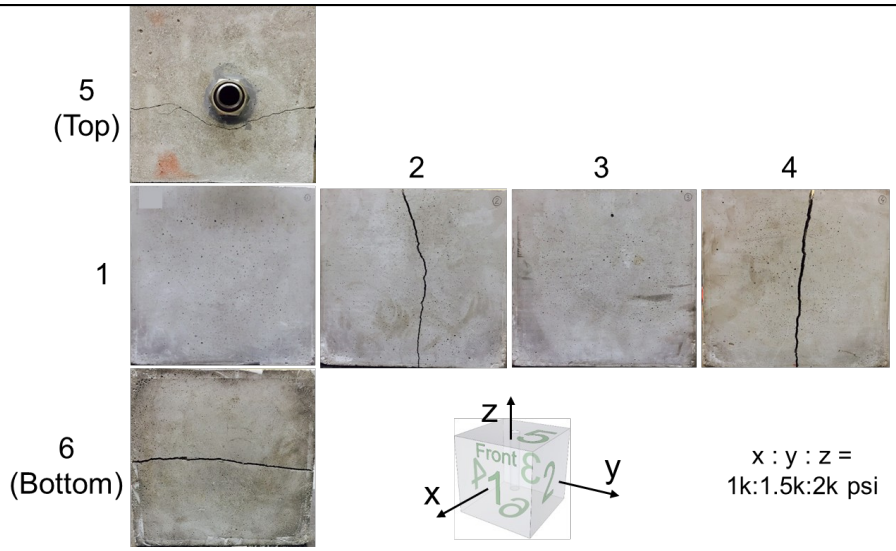

(b) Specimen #21

Figure 8—Block surfaces after breakdown fracturing (using gaseous nitrogen) without LN stimulation. Note that fractures are located along the y-z plane (i.e., the plane with the principal stress and intermediate stress directions). Breakdown fractures occurred suddenly without any pre-leaking.

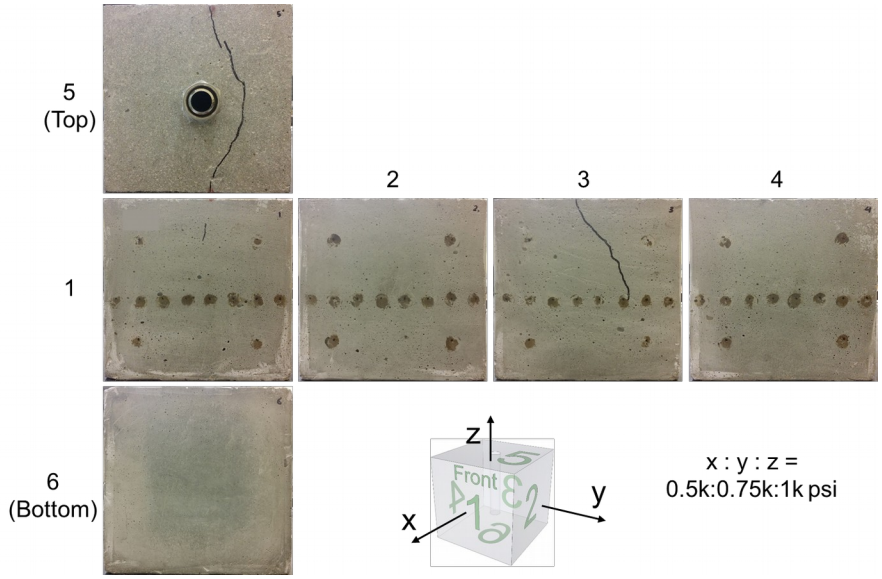

(a) Specimen #19

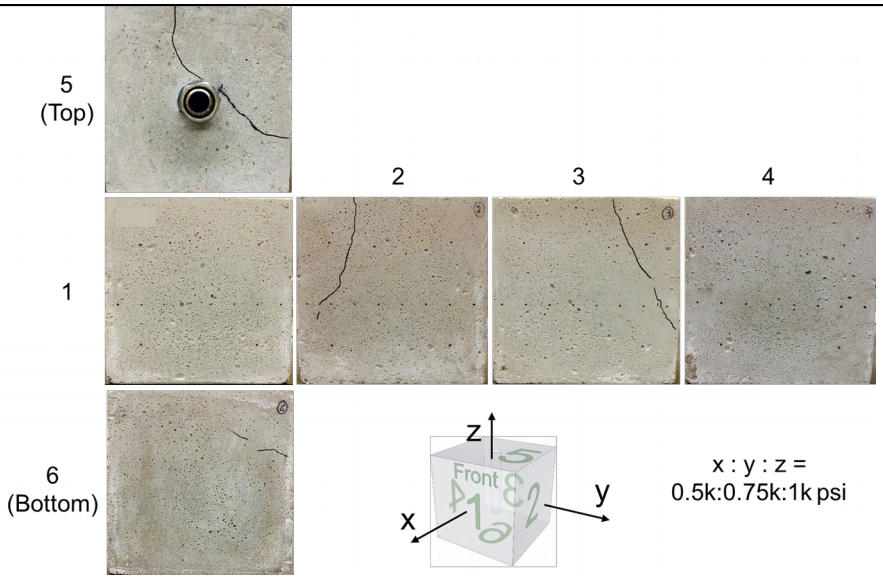

(b) Specimen #20

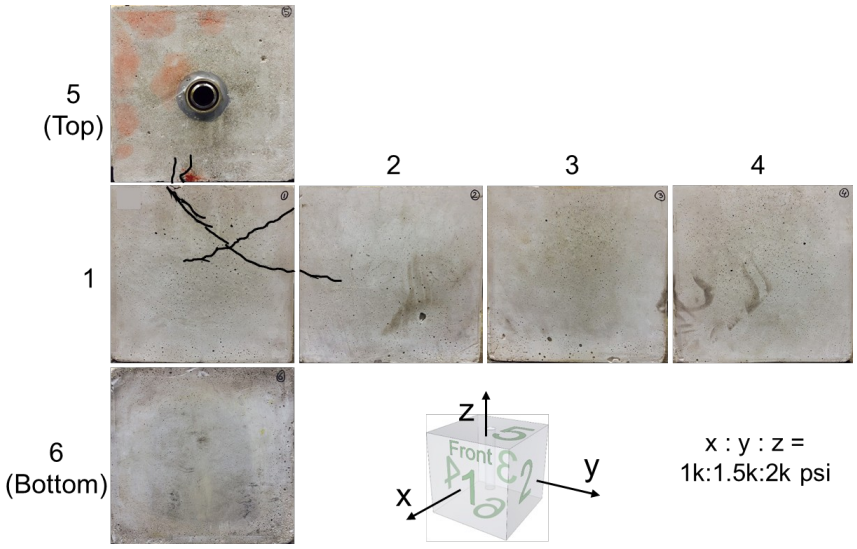

(c) Specimen #22

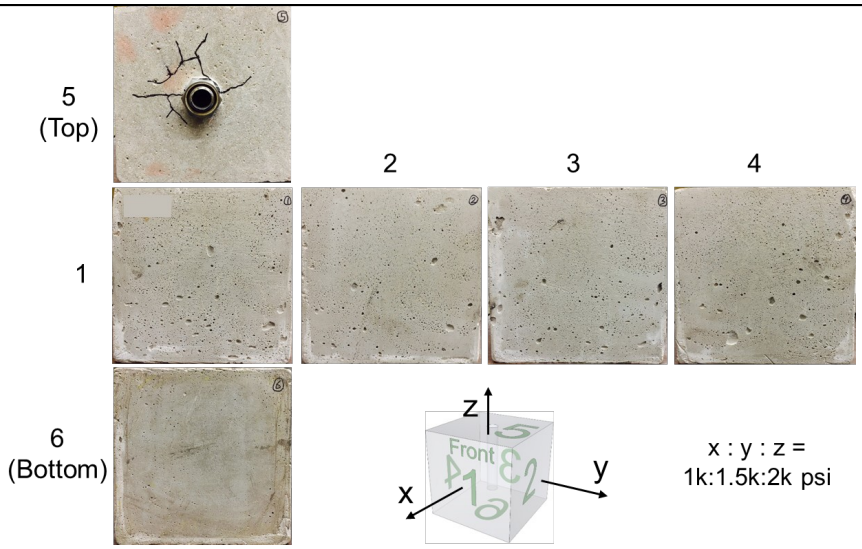

(d) Specimen #23

Figure 9—Block surfaces after breakdown following LN stimulations. Fractures do not follow y-z plane, and are in rather arbitrary directions (a & b), or occurred only locally (c & d). The breakdown occurred more gradually with significant pre-leaking.

Cryogenic fractures as "seed fractures" for pressure-induced fracturing

After the breakdown tests, specimens were separated along the major fractures, and fracture surfaces were visually inspected. There were clear discontinuities that indicate that part of the fracture surfaces was cryogenically induced and part of the fracture surfaces was opened up by the high P_{BD}. The surfaces of the cryogenically opened fractures are adjacent to the borehole, and are slightly rounded, while the surfaces opened up by high gas pressure are straighter (Figure 10). This sequence suggests that cryogenic stimulation created "seed" fractures that did not fully extend to the external surface (except the top portion). These seed fractures, however, significantly lowered the P_{BD}, as presented earlier. Creation of seed fractures was likely responsible for the pre-leaking observed during applications of breakdown pressures to the boreholes. It should be noted that many sets of seed fractures may have been generated. Only a major one, however, was activated by the breakdown pressure and eventually led to the separation of the specimen. Having multiple seed fractures starting from and adjacent to the borehole is favorable from the production's point of view because they improve the permeability near the borehole and not just along the primary fracture. When the specimen was not treated with LN, only a sharp straight fracture formed from the borehole to the block surfaces; no discontinuities in the surface morphology were observed (Figure 11).

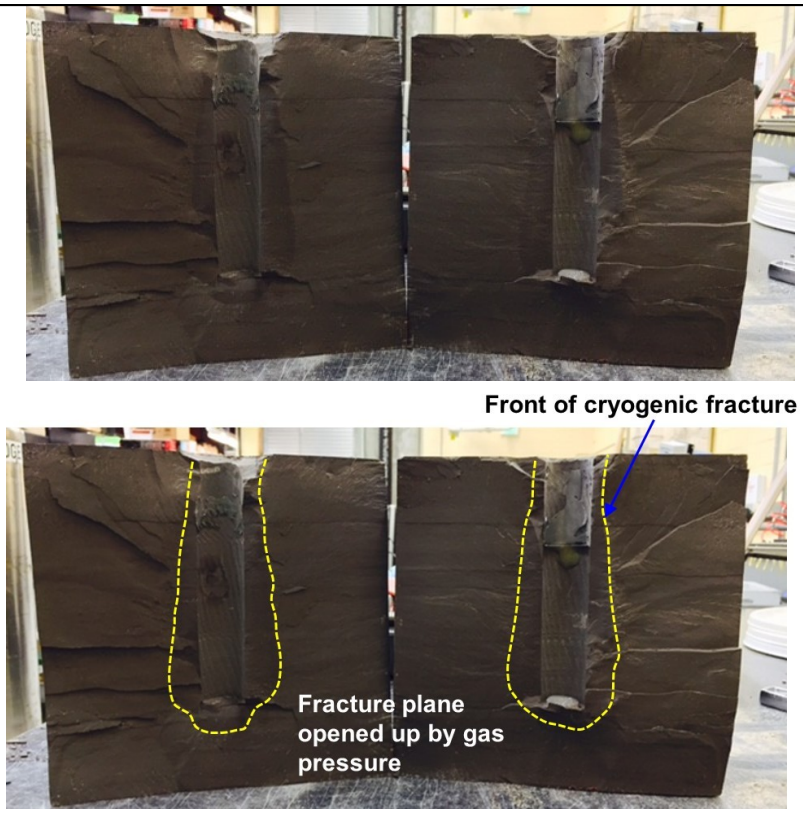

(a)

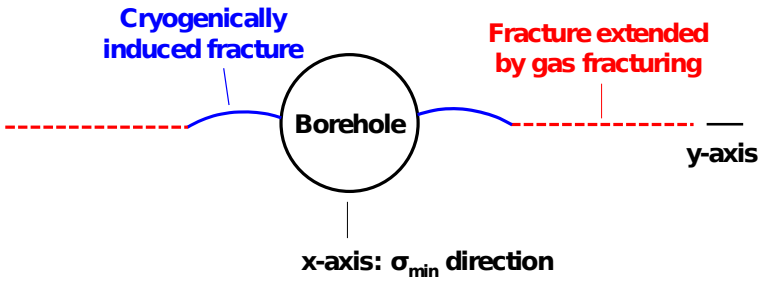

(b)

Figure 10—Fracture plane after breakdown fracturing of LN treated shale specimen (Specimen #S2). (a) Yellow dotted lines show the front of cryogenically created fractures. (b) Depiction of fractures at the midheight of the shale block: Slightly curved nature of cryogenically induced fractures and straight fractures extended by gas fracturing.

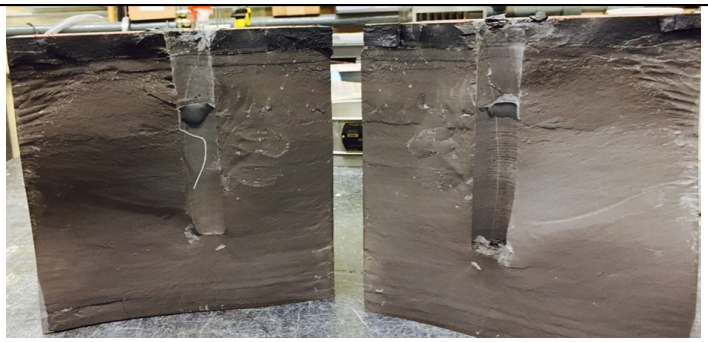

Figure 11—Fracture plane after breakdown fracturing of the untreated shale specimen (Specimen #S4).

Permeability changes

After each treatment procedure, enhancements in the permeability were assessed by borehole pressure decay tests.

Permeability increase due to cryogenic treatment

Permeation (pressure decay) profiles clearly show that low- and high-pressure liquid nitrogen flow increased the permeability of treated specimens. In one test, LN flowed under low pressure for 36 min resulted in a significant permeability increase (Figure 12a) indicated by a more rapid pressure decay. Three cycles of higher-pressure LN flows under triaxial loading also led to significant permeability enhancements. We observed that repeated cryogenic stimulations increased permeability further, indicating that each LN treatment cycle created new fractures and/or widened existing fractures. Figure 12b is an example of a higher-pressure LN flow test, where greater permeability was achieved after each brief LN cycle.

Effect of temperature

We also observed the effect of temperature on the permeability of the specimen that experienced cryogenic stimulation. Permeability decreased when the specimen returned to the room temperature after the low-pressure treatment (Figure 12a) and after the third high-pressure LN flow (Figure 12c). When the temperature of the specimen was low, the specimen was in the state of local thermal contraction near the borehole and fractures should remain open around the borehole. As the specimen warmed, the thermally induced stresses relaxed, and fractures closed reducing the permeability of the specimen.

In contrast, in untreated specimens or weakly treated specimens, the permeability was lower when the specimen was at a lower temperature and increased when it returned to the room temperature. In other words, if no fracture exists near the borehole, permeability is lower at a lower temperature. At low temperature, the specimen is under thermal contraction, and consequently, the pore sizes are reduced, and perhaps the natural fracture widths are also smaller. This behavior was sometimes observed after the first cycle of brief high-pressure flow through.

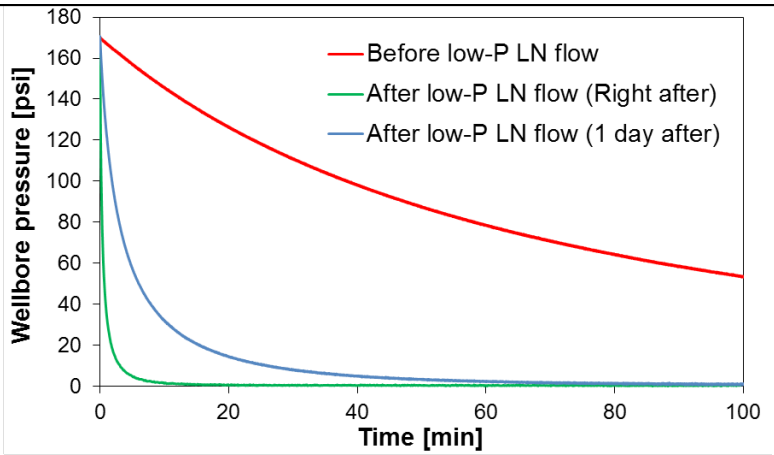

(a) Effect of low-pressure LN flow on permeability (specimen unconfined except 60-psi vertical loading). More rapid pressure loss indicates higher permeability.

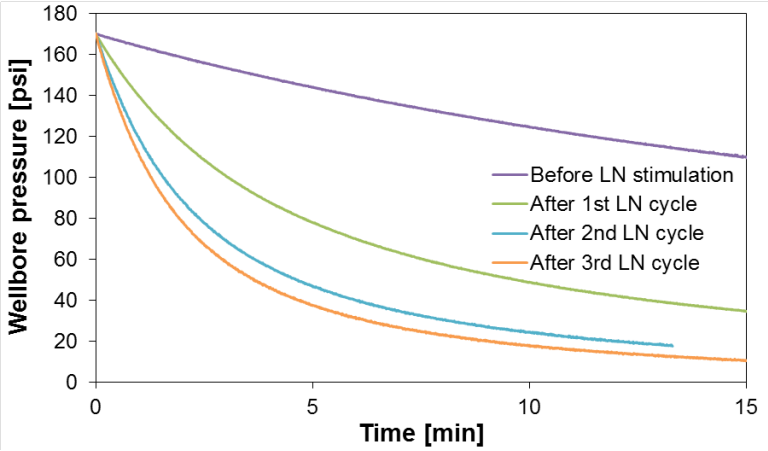

(b) Effect of repeated high-pressure LN flow on permeability (under confining stresses).

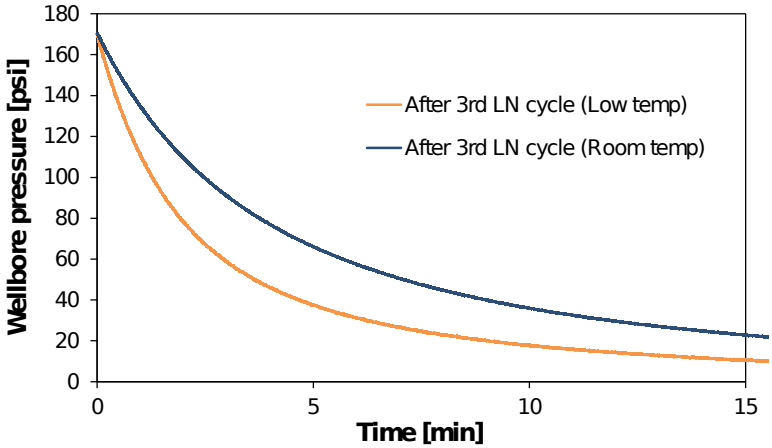

(c) Effect of specimen temperature on permeability (under confining stresses).

Figure 12 — Effect of cryogenic treatment on permeability changes (Specimen #S1).

Acoustic wave signature

Changes in the specimens' ability to transmit acoustic waves before and after stimulations were examined. Acoustic waves were measured between Faces 1&3 and 2&4 (pairs of opposing faces) (Figure 13a). Figure 13b shows the twelve locations of the acoustic actuators and receivers on a specimen surface. We observed that acoustic velocities and amplitudes decrease (original amplitudes not shown) after cryogenic treatments, indicating fracture creation in the specimens. For shale specimens, we also observed the effect of layering on the velocities and attenuations.

Acoustic results before breakdown tests generally agree with the fracture profile after the breakdown tests. In particular, velocities and amplitudes significantly decreased in specimens where a major fracture was identified (Figures 14 and 15 locations #5-#10). Because waves interrogate the entire specimen, changes in wave signals (wave velocity and amplitude) reflect the average properties of the specimen; however, the effect of the locality of the sensor is significant. Signals compared with their full waveforms show that the global frequency of the signals became lower after cryogenic stimulations at nearly all measurement spots.

Changes in P-wave velocities are summarized in Figure 16. Lower velocities near the edges (#1 & 8) and center (#4 & 5) show the effects of boundaries and borehole cavity. In rare cases, velocity slightly increased at a particular location, which suggests a local compressed zone. Such a signal usually takes place in the corner. These acoustic measurements suggest that they can be used to detect fractures near the borehole that are otherwise invisible to naked eyes and with X-ray computed tomography CT scans.

CT was attempted with a CT scanner with a voxel size 0.2mm× 0.2mm× 0.2mm but failed to provide enough resolution to identify cryogenically-induced fractures near the wellbore. Proppants were not used in this study. Fractures created by cryogenic stimulations tended to close as a specimen warmed. No self-propping mechanisms were observed in the laboratory-sized specimens of concrete, shale, and sandstones.

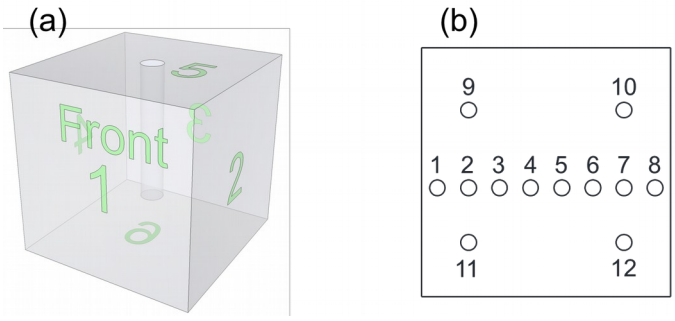

Figure 13—Waves measured along Face 1 & 3 and 2 & 4. (a) Face numbering convention. (b) Measurement locations on a surface.

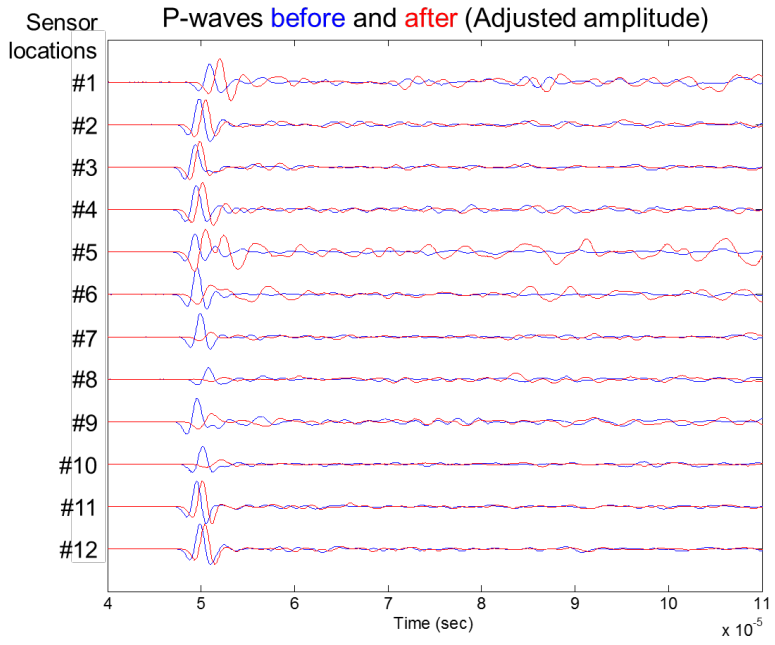

Figure 14—P-wave signals (adjusted amplitude) across Faces 2-4 before and after stimulation (Specimen #19).

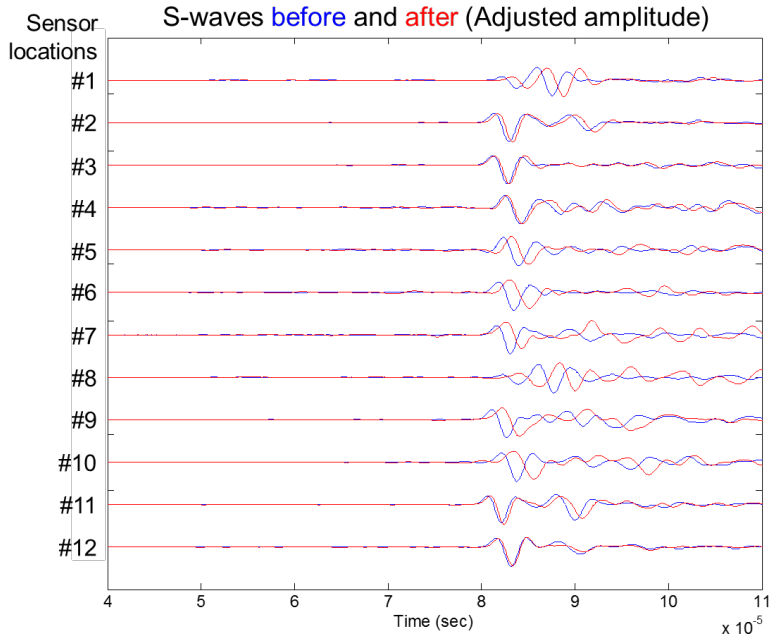

Figure 15—S-wave signals (adjusted amplitude) across Faces 2-4 before and after stimulation (Specimen #19).

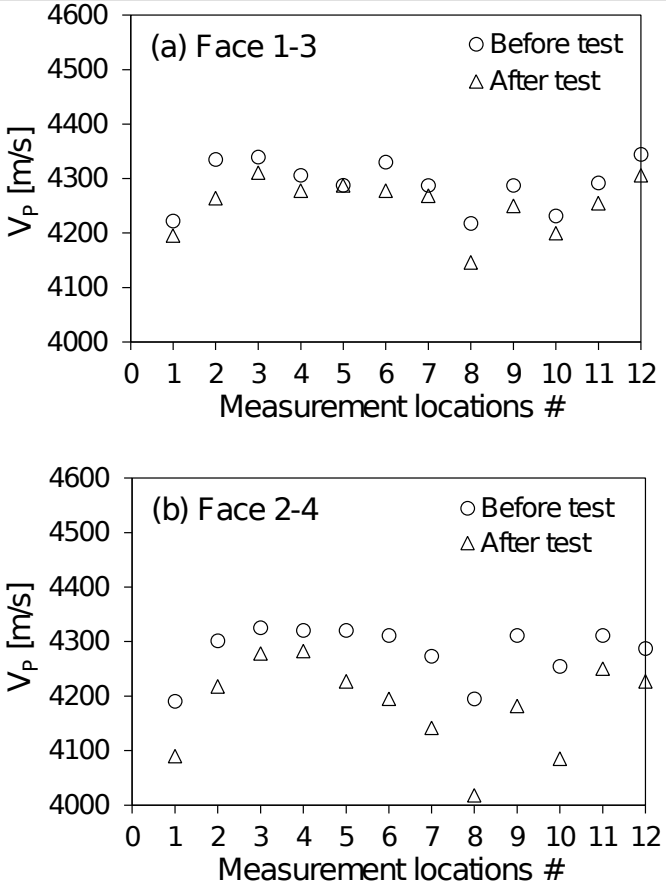

Figure 16—P-wave velocity comparisons – before and after treatments (Specimen #19).

Table 2—Matrix of cryogenic fracturing experiments performed under triaxial confining stresses.

Specimen #	Specimen type	Stresses (x:y:z) [psi]	Test procedure	Measured P_{BD} [psi]	Notes
16	Concrete	500:750:1000	Fracturing by GN	583#	# Weakness created near the casing
17	Concrete	500:750:1000	Fracturing by GN	1180	
18	Concrete	500:750:1000	Low-pressure LN flow (30 min) + Fracturing by GN	685	
19	Concrete	500:750:1000	High-pressure LN flow + Fracturing by GN	778	
20	Concrete	500:750:1000	High-pressure LN flow + Fracturing by GN	759	
21	Concrete	1000:1500:2000	Fracturing by GN	1317	
22	Concrete	1000:1500:2000	Low-pressure LN flow (30 min) + Fracturing by GN	-	
23	Concrete	1000:1500:2000	High-pressure LN flow + Fracturing by GN	1094	
S1 (24)	Shale 1	1000:1500:2000	Low-pressure LN flow (40 min)		CT scanned before & after the LN test.
			High-pressure LN flow	1394	3 LN treatment cycles.
S2 (25)	Shale 2	1000:3000:4000	High-pressure LN flow (1st round)	1417	3 LN treatment cycles for each round. LN flowed until getting similar decay curves at last runs.
			High-pressure LN flow (2nd round)		
S3 (26)	Shale 3	1000:1500:2000	Low-pressure LN flow (40 min)		Pressure decay before & after show a permeability enhancement
			High-pressure LN flow	168	Fractured at early stage when doing pressure decay before testing & before loading (fractured at 180 psi)
S4 (27)	Shale 4	1000:1500:2000	Fracturing by GN	2439	
SS1	Sandstone	1000:1500:2000	High-pressure LN flow	219	Fractured during pressure decay test when σ_z = 60 psi
SS2	Sandsto	σ_z = 60 psi	Fracturing by GN	689	

	ne				

Breakdown pressure and thermal stress analysis

Breakdown pressures are affected by thermo-poroelasticity of near-wellbore formation. Coupled temperature and pore pressure equations were solved for different formation permeability conditions - for permeable and impermeable boundaries – under non-hydrostatic stresses (Chen and Ewy 2005, Li et al. 1998, Wu et al. 2010, Detournay and Cheng 1988). In this study, a simple estimation of expected P_{BD} for untreated specimens is performed using Equation 1, which assumes that the breakdown occurs when the effective Terzaghi tensile stress reaches the rock tensile strength in the wall of the wellbore (Guo et al. 1993, Hubbert and Willis 1957). No initial pore pressure exists in the rock in this study, and rock is assumed impermeable. The breakdown pressure (P_{BD}) is:

$$P_{BD}=3\sigma_h-\sigma_H+\sigma_t \qquad \text{Equation 1}$$

In the equation, σ_H and σ_h are maximum and minimum horizontal stresses, respectively, and σ_t is tensile strength. The calculated P_{BD} are listed in Table 3 and compared to the measured values.

During the cryogen flow through a borehole, large thermal stresses are induced by rapid cooling at the wellbore surface and near wellbore. Estimates of the changes in the tangential thermal stress component induced by thermal gradient on the wellbore wall are provided by Equation 2 assuming fractures are not created (Zhang et al. 2014, Zoback 2010, Tarasovs and Ghassemi 2011).

$$\sigma_{max}^{\Delta T}=\frac{E}{1-\nu}\alpha\cdot\Delta T \qquad \text{Equation 2}$$

In the equation, ΔT is temperature difference, α is coefficient of linear thermal expansion (K^{-1}), E is static Young's modulus (GPa), and ν is Poisson's ratio. From the properties in Table 1 and ΔT = 200 °C that is reasonably assumed, we obtain $\sigma_{max}^{\Delta T}$ = 90MPa for the concrete and 125MPa for the shale, which are significantly larger than the materials' tensile strengths. These indicate that fractures will occur in all cases in the absence of confining stresses.

The amount of mobilized thermal stresses required to initiate fractures by cooling temperature changes in a specimen under confining stress and anisotropy relevant to this study can be estimated (Equation 3). During the low-pressure thermal stimulations, the magnitudes of borehole pressure are negligible.

$$\sigma_{mobilized}^{\Delta T}=3\sigma_h-\sigma_H+\sigma_t \qquad \text{Equation 3}$$

For σ_h=1000 psi and σ_H=1500 psi, thermal stresses mobilized to initiate fractures are $\sigma_{mobilized}^{\Delta T}$ = 13.2 MPa for the concrete and 18.8 MPa for the shale, which are well below $\sigma_{max}^{\Delta T}$ estimated above.

Concrete specimen #17 was fractured by GN pressure without LN treatment. The calculated P_{BD} of the specimen is close to that measured from the test (Table 3). The P_{BD} for specimen #17 can, therefore, be used as a baseline P_{BD} for the other tests using concrete specimens. The table shows that concrete specimens #18-20, which were treated with LN with different procedures, have lower P_{BD}'s than that of

specimen #17 and that calculated from Equation 1. P_{BD} of specimen #18 was reduced by 42%, while specimens #19 and #20 were reduced by ~36%. Note that specimen #18 was stimulated by low-pressure LN flow for 30 minutes under low pressure, which may be more substantial stimulation than single-cycle high-pressure LN flow that was applied to specimens #19 and #20. Concrete specimens #21-23 were tested under higher triaxial loadings than #16-20. Specimen #23 was treated, and its P_{BD} value was lower by 43% than the calculated P_{BD}. P_{BD} for specimen #21 (untreated) is higher than the P_{BD} of Specimen #23, but found to be lower than the calculated P_{BD} by 31%. Some possibilities of the difference between the P_{BD} of the untreated specimen and the calculated may include damages during the higher loading and inhomogeneities in the concrete created during fabrication.

Shale #S1 and #S4 were tested under the same triaxial loading as concrete specimens #21 - #23. S1 was treated with LN and shows a P_{BD} reduced by 43% compared to the P_{BD} for S4, which was not treated with LN. Shale #S2 was tested under the high-stress anisotropy, making its calculated P_{BD} low due to the high maximum horizontal stress σ_H (Equation 1). Exceptionally, the measured P_{BD} for shale #S2 is found to be slightly higher than the calculated P_{BD}. Overall, LN treatments create cracks to the wellbore surface and reduce the P_{BD} needed to initiate the fracture.

Table 3—Comparison between measured P_{BD} and calculated P_{BD}.

Specimen #	Specimen type	Stresses (x:y:z) [psi]	Measured P_{BD} [psi]	Calculated P_{BD} [psi] by Eq. 1	Mea.P_{BD}/Cal. P_{BD}
16	Concrete	500:750:1000	*583*†	1168	0.5
17	Concrete	500:750:1000	1180	1168	1.01
18	Concrete*	500:750:1000	685	1168	0.58
19	Concrete*	500:750:1000	778	1168	0.67
20	Concrete*	500:750:1000	759	1168	0.65
21	**Concrete**	**1000:1500:2000**	**1317**	**1918**	**0.68**
22	**Concrete***	**1000:1500:2000**	**-**	**1918**	**-**
23	**Concrete***	**1000:1500:2000**	**1094**	**1918**	**0.57**
S1	Shale*	1000:1500:2000	1394	2726	0.51
S2	Shale*	1000:3000:4000	1417	1226	1.15
S4	Shale	1000:1500:2000	2439	2726	0.89

*LN treated.
†Breakdown fractures concentrated near the casing.

Discussion

Laboratory tests and field delivery of liquid nitrogen.

Boundary and scale effects are inherent in laboratory-sized specimens. Our specimen size (8") is limited by the capacity of the triaxial frame to apply reasonable reservoir stresses, and smaller 1"-diameter central wellbores were chosen to maintain sufficient thermal gradient and generate thermal stress as fractures initiate and propagate. The fracture traces observed in Cha, Alqahtani, Yao, Wang, et al. (2016) using transparent specimens with a similar size show that a set of radial and vertical thermal fractures were created and propagate outward due to locally developed thermal stresses. As the fractures approach boundaries, however, the fracture growth rate tended to slow down. Tarasovs and Ghassemi (2014) revealed that similar quasi-uniform distances between fractures, and self-similarity and scaling of thermal shock fractures. Haimson and Zhao (1991) and Ito et al. (1990) showed that P_{BD} tend to decrease with increasing wellbore diameter, and laboratory tests in boreholes greater than 20mm in diameter yield P_{BD} essentially unaffected by borehole diameters and are usable in interpretation of field data.

Significant amounts of liquid nitrogen may be needed per stimulation in the field. In this study, up to 25 liters of LN was consumed for low-pressure flow of LN through 1" wellbore for 30 minutes. In the field, assuming a wellbore of 5" inner diameter, 5-hour low-pressure flow in an open borehole, considering the cross section area and similar flow rate, the volume 6250 liters or 1650 gallons may be estimated. However, heat loss due to long delivery to wells and longer isolated zones will significantly increase this figure depending on site characteristics and stimulation schemes. On the other hand, LN is among the cheapest cryogen, as low as $0.06/liter and available in large truckload quantities (Sheahen 1994, Fan 2007). LN price increases with distance from a condensing plant, and, beyond a certain distance, LN may be manufactured on site and will still be relatively inexpensive (Fan 2007).

In field applications, heat loss and integrity of transport lines and casing may be issues to overcome for delivery of liquid nitrogen to the downhole environment. For both vertical and horizontal wells, the injection pipe string should have minimum contact with the casing in order to not affect casing integrity and to minimize heat loss. The injection pipes should maintain sufficient strength and structural integrity at cryogenic temperature. Suitable materials include stainless steel, brass, and fiberglass (Wilson et al. 1995). Fiberglass has the merit of a lower cost, lighter weight, and lower thermal conductivity, and for these reasons was tried in field tests (McDaniel et al. 1997). Due to inherent heat loss, the delivery pipe should be cooled before the cryogen can flow in a liquid state. From our laboratory experience, faster flow rate helps overall thermal flux, reducing the relative rate of heat loss. Nevertheless, heat loss is inevitable and may increase at greater depth. In-situ cooling may be a potential alternative, such as by Joule-Thomson process, which requires additional development.

Comparisons with thermal stresses during hydraulic fracturing.

In hydraulic fracturing using water, thermal effects from injection of a cold fracturing fluid further stimulate the hydraulic fractures. The temperature difference between injected water and downhole formation of oil/gas wells at typical depth is 20-60°C (but can be much greater for an enhanced geothermal field), considerably less than the range 200-250°C at cryogenic fracturing. In

addition, in water fracturing, water is injected under pressure rather than flowing through. Fractures propagate and/or water permeates into the formation. Under these conditions, the fluid temperature equilibrated with the formation quite quickly (Salimzadeh et al. 2016). Nevertheless, intensive cooling accelerates the growth speed when the fluid pressure imposed is fixed. The increased opening induced by the thermal effect allows the fluid pressure to penetrate along the fracture (Wu et al. 2016).

In water fracturing, water pressure dominates the fracturing process, while the thermal stresses induced by the temperature differences help pressure fracturing. The hydraulic-thermal coupled load may lower fracture pressure due to contribution of thermal stress as seen in this paper. Injection of cool water can reduce earth stresses around injection wells substantially, causing them to fracture at pressures considerably lower than would be expected in the absence of the thermoelastic effect (Perkins and Gonzalez 1985, Wu et al. 2016).

Hydraulic fractures tend to grow normal to the minimum horizontal stress. Injection of cold fracturing water into reservoir rock induces thermal cracks perpendicular to hydraulic fracture, creating a jointed fracture system. The heat transfer cools down the zone neighboring the fracture and the rock shrinks parallel to hydraulic fracture length (Enayatpour and Patzek 2013, Perkins and Gonzalez 1985).

Numerical studies show that a thermal shock during hydraulic fracturing can create small cracks, which might extend to intersect natural fractures or be extended by subsequent hydraulic fracturing. Initially many small thermal cracks are created, however only a few of them can grow far away from the hydraulic fracture. Growth of multiple thermal cracks improves the productivity; thermal cracks in rock have the potential to improve the productivity of wells in tight formations by 20% (Enayatpour and Patzek 2013). During hydraulic fracturing, thermally induced stress may open cemented natural fractures. Despite small sizes of these fractures, their large numbers may increase formation contact area significantly (Dahi Taleghani et al. 2014).

Influence of fracturing fluid properties.

The rheology of fracturing fluid have a strong influence on the creation and propagation of the fractures (Bohloli and De Pater 2006). Slickwater treatments use low-viscosity fluids pumped at high rates to generate narrow, complex fractures with low-concentrations of propping agent (King 2010). For conventional bi-wing fractures, the fracturing fluid must be sufficiently viscous to transport higher proppant concentrations. These treatments are often pumped at lower pump rates and may create wider fractures. When a lower-viscosity fluid is used, the fluid infiltrates into the fracture more readily. Crack initiation pressure and breakdown pressure for the low viscosity fluid are lower than those for high viscosity fluid (Shimizu et al. 2011, Zhang et al. 2017). Increasing the viscosity of the fracture fluid decreases the local extent of the propagation of the microseismic cloud (Hosseini et al. 2014).

Unlike pressure-based fracturing, the fractures created during the low-pressure cryogenic flow are due to purely thermal shock. In this case, thermal properties of the cryogen gain importance as they affect heat transfer (Table 4). Fluid rheology may have a minimum effect on fracture creation, yet nitrogen may flow readily through created fractures due to its low viscosity in either gas or liquid

states (Table 4). Under the higher-pressure cryogenic flow where borehole pressure aids fracture generation, fracture creation may be affected by rheology of nitrogen. Still, in the early stage of the heat flow, a gas film lies between surface and liquid nitrogen because liquid nitrogen immediately boils when the rock surface is much hotter. On the other hand, gas nitrogen was used during breakdown fracturing process of treated and untreated specimens. Similarly, in the field, the use of nitrogen gas pressure after a thermal stimulation may be preferred for propagating fractures, due to lack of interaction of nitrogen with formation, which is one of purposes of cryogenic fracturing.

Fracturing by nitrogen gas demonstrated success in reservoirs found sensitive to liquid (Freeman et al. 1983). Yet, width reductions in unpropped fractures typically occur in the early stage of production. In the Ohio Shale Formation, nitrogen gas fracturing, even without proppants, outperformed conventional stimulation systems (Abel 1981). Nitrogen is inert, and problems of clay swelling, clay migration, or oil and water emulsions are eliminated (Gottschling and Royce 1985). Cost is normally less than conventional hydraulic fracturing, and also cheaper than other gases (Clancy and Gilchrist 1983, Gottschling and Royce 1985).

The viscosities of gas and liquid nitrogen are respectively 1/50 and 1/6.3 of that of water (Table 4). One implication of low viscosity of fracturing fluids is low proppant-carrying ability. Proppants could be used with gas nitrogen and cryogens under high velocity injection (Gottschling and Royce 1985, Gupta and Bobier 1998). As discussed in Introduction section, ultralight proppant may be used with LN and GN, and gelled CO_2 may be used as a carrier fluid.

Table 4—Some properties of injection fluids.

	Water*	Gas nitrogen*	Liquid nitrogen†
Viscosity [cP]	1.002	1.76×10^{-2}	0.158
Density [g/ml]	0.998	0.0012	0.807
Surface tension [dyn/cm] (against air)	72.8	-	8.85
Specific heat [kJ/(kg•K)]	4.18	1.04	2.04
Thermal conductivity [W/(m•K)]	0.591	0.025	0.140

* Normal temperature and pressure (20 °C and 1 atm).
† 77K and 1 atm.

Conclusions

Cryogenic fracturing was investigated as a well stimulation technique. An integrated experimental system was designed for the first controlled laboratory cryogenic fracturing study at wellbore conditions under true-triaxial loading. We conducted cryogenic fracturing tests using laboratory rock blocks and found that fractures are clearly generated by LN flow through a borehole under low and high flow pressure. The effectiveness of cryogenic fracturing processes depends on cryogen flow pressure/rate, treatment time and cycles, rock properties, and triaxial loading conditions.

Cryogenically driven fractures were initiated from the borehole surfaces and propagated adjacent to the boreholes to some extent, indicating that borehole pressurization may be needed to induce deeper fracture penetration. However, P_{BD}

levels are significantly lowered by cryogenic stimulation. This reduction of P_{BD} levels is possible by the formation of seed fractures created during cryogenic stimulation in the borehole. The cryogenic stimulation schemes applied in this study are capable of reducing P_{BD} of concrete and shale blocks by about 40%.

In cryogenically stimulated specimens, the direction of fracture propagation upon applying breakdown fracture pressure can deviate from the directions theoretically expected in specimens under triaxial stress anisotropy. Apparently, cryogenic stimulations alter local stress fields around the wellbore, and could lead to tortuous fractures. Very high-stress anisotropy, however, may overpower the cryogenic stimulation effect and result in conventionally expected direction of breakdown fractures - perpendicular to the minimum stress direction.

The profiles of borehole pressure decay obtained before and after each stage of stimulation show that low- and high-pressure liquid nitrogen flows increase the permeability of treated specimens. Multiple treatments in shale blocks demonstrate that increasing the number of stimulations increases permeability possibly by furthering fracture propagation and creating new fractures. We also observed the effect of temperature at the time of measurements. As temperature returns to ambient, the cryogenically-generated fractures tend to close, resulting in permeability reduction. Acoustic measurements confirm that liquid nitrogen stimulations generate micro-fractures inside the blocks, which will increase the matrix permeability.

The understanding obtained in this study may be further developed for field-scale applications. The cryogenic fracturing technique might reduce water usage and minimize the formation damage. Cryogenic fracturing could also be used in combination with other conventional stimulation technologies. In particular, the technique may help in the field to reduce the P_{BD} by creating seed fractures prior to a pressure-based treatment.

Acknowledgements

Support for this research was provided by Research Partnership to Secure Energy for America (RPSEA) (Grant no.10122-20). This work was also supported by Fundation CMG. Kneafsey performed work at Lawrence Berkeley National Laboratory (LBNL) of the US Department of Energy (DOE) under Contract No. DE-AC02-05CH11231 with funding provided by RPSEA through the Ultra-Deepwater and Unconventional Natural Gas and Other Petroleum Resources program authorized by the US Energy Policy Act of 2005. RPSEA is a nonprofit corporation whose mission is to provide a stewardship role in ensuring the focused research, development, and deployment of safe and environmentally responsible technology that can effectively deliver hydrocarbons from domestic resources to the citizens of the US. RPSEA, operating as a consortium of premier US energy research universities, industry, and independent research organizations, manages the program under a contract with DOE’s National Energy Technology Laboratory.

Nomenclature

μ = gas viscosity (cp)
σ_{avg} = the average in-situ stresses (psi)
σ_h = Minimum horizontal stresses (psi)
σ_H = Maximum horizontal stresses (psi)

c_f = formation (shale) compressibility (1/psi)
h = interested zone length (ft)
m = the slope (psi/cycle)
q = gas flowrate (scf/day)
B = gas formation volume factor (RB/STB)
G = giga
K = permeability after loading (md)
K_o = permeability before loading (md)
M = mega
P_{BD} = Breakdown pressure (psi)
T_o = Tensile strength (psi)

SI metric conversion factors

inch × 2.54 E-01 = m
g/cm^3 × 1.0 E+03 = kg/m^3
md × 1.01325 E+12 = m^2
psi × 1.45038 E-04 = Pa
$(T_{\circ F}+459.67)/1.8 = T_{\circ C}$

References

Abel, J. C. 1981. Application of Nitrogen Fracturing in the Ohio Shale. Proc., the 1981 SPE Eastern Regional Meeting, Columbus, Ohio, November 4-6, 1981.

ASTM D3967 Standard Test Method for Splitting Tensile Strength of Intact Rock Core Specimens. 2008.

ASTM C192/C192M Standard Practice for Making and Curing Concrete Test Specimens in the Laboratory. 2014a.

ASTM D7012 Standard Test Methods for Compressive Strength and Elastic Moduli of Intact Rock Core Specimens under Varying States of Stress and Temperatures. 2014b.

Beugelsdijk, L., C. De Pater, K. Sato. Experimental hydraulic fracture propagation in a multi-fractured medium. Society of Petroleum Engineers.

Bohloli, B., C. De Pater. 2006. Experimental study on hydraulic fracturing of soft rocks: Influence of fluid rheology and confining stress. *Journal of Petroleum Science and Engineering* **53** (1): 1-12.

Cha, M., N. Alqahtani, B. Yao, L. Wang, X. Yin, Y. Wu, T. Kneafsey. 2016. Studying cryogenic fracturing process using transparent specimens. Proc., The 1st International Conference on Energy Geotechnics, August 29-31, 2016, Kiel, Germany, 211-216.

Cha, M., N. B. Alqahtani, B. Yao, X. Yin, Y. S. Wu, T. J. Kneafsey. 2016. Development of laboratory system for cryogenic fracturing study. Proc., The 1st International Conference on Energy Geotechnics, Kiel, Germany, 381-388.

Cha, M., N. B. Alqahtani, X. Yin, T. J. Kneafsey, B. Yao, Y.-S. Wu. 2017. Laboratory system for studying cryogenic thermal rock fracturing for well stimulation. *Journal of Petroleum Science and Engineering* **156**: 780-789.

Cha, M., G. C. Cho. 2007. Compression wave velocity of cylindrical rock specimens: engineering modulus interpretation. *Japanese Journal of Applied Physics Part 1-Regular Papers Brief Communications & Review Papers* **46** (7B): 4497-

4499.
Cha, M., G. C. Cho, J. C. Santamarina. 2009. Long-wavelength P-wave and S-wave propagation in jointed rock masses. *Geophysics* **74** (5): E205-E214.
Cha, M., X. Yin, T. Kneafsey, B. Johanson, N. Alqahtani, J. Miskimins, T. Patterson, Y.-S. Wu. 2014. Cryogenic fracturing for reservoir stimulation – Laboratory studies. *Journal of Petroleum Science and Engineering* **124**: 436-450.
Chen, G., R. T. Ewy. 2005. Thermoporoelastic effect on wellbore stability. *SPE Journal* **10** (02): 121-129.
Clancy, J., R. Gilchrist. 1983. Nitrogen injection applications emerge in the rockies. Proc., SPE Rocky Mountain Regional Meeting.
Dahi Taleghani, A., M. Ahmadi, W. Wang, J. E. Olson. 2014. Thermal reactivation of microfractures and its potential impact on hydraulic-fracture efficiency. *SPE Journal* **19** (05): 761-770.
Detournay, E., R. Carbonell. 1997. Fracture-mechanics analysis of the breakdown process in minifracture or leakoff test. *SPE production & facilities* **12** (03): 195-199.
Detournay, E., A.-D. Cheng. 1988. Poroelastic response of a borehole in a non-hydrostatic stress field. *International Journal of Rock Mechanics and Mining Sciences & Geomechanics Abstracts* **25** (3): 171-182.
Enayatpour, S., T. Patzek. 2013. Thermal Shock in Reservoir Rock Enhances the Hydraulic. Proc., Unconventional Resources Technology Conference (URTEC).
Fan, K. 2007. Price Of Liquid Nitrogen. The Physics Factbook (hypertextbook.com/facts/2007/KarenFan.shtml).
Fenghour, A., W. A. Wakeham, V. Vesovic. 1998. The Viscosity of Carbon Dioxide. *Journal of Physical and Chemical Reference Data* **27** (1): 31-44.
Freeman, E. R., J. C. Abel, C. M. Kim, C. Heinrich. 1983. A stimulation technique using only nitrogen. *Journal of Petroleum Technology* **35** (12): 2,165-2,174.
Gottschling, J., T. Royce. 1985. Nitrogen gas and sand: a new technique for stimulation of Devonian shale. *Journal of petroleum technology* **37** (05): 901-907.
Grundmann, S. R., G. D. Rodvelt, G. A. Dials, R. E. Allen. 1998. Cryogenic Nitrogen as a Hydraulic Fracturing Fluid in the Devonian Shale. SPE-51067-MS. Proc., SPE Eastern Regional Meeting, Pittsburgh, Pennsylvania.
Guo, F., N. R. Morgenstern, J. D. Scott. 1993. Interpretation of hydraulic fracturing breakdown pressure. *International Journal of Rock Mechanics and Mining Sciences & Geomechanics Abstracts* **30** (6): 617-626.
Guo, T., S. Zhang, Z. Qu, T. Zhou, Y. Xiao, J. Gao. 2014. Experimental study of hydraulic fracturing for shale by stimulated reservoir volume. *Fuel* **128**: 373-380.
Gupta, D. V. S., D. M. Bobier. 1998. The history and success of liquid CO_2 and CO_2/N_2 fracturing system. SPE-40016-MS.
Haimson, B. C., Z. Zhao. 1991. Effect of Borehole Size And Pressurization Rate On Hydraulic Fracturing Breakdown Pressure. Proc., The 32nd U.S. Symposium on Rock Mechanics (USRMS), 10-12 July, Norman, Oklahoma.
Hosseini, S. M., C. W. Neuhaus, F. Aminzadeh. 2014. Effect of Fluid Rheology and Reservoir Compressibility on Microseismicity during Hydraulic Fracturing. Proc., SPE Annual Technical Conference and Exhibition.
Hubbert, M. K., D. G. Willis. 1957. Mechanics of hydraulic fracturing. *Trans. Am. Inst. Min. Engrs.* **210**: 153-168.

Ito, T., K. Hayashi, H. Abe. 1990. Scale effect in breakdown pressure of hydraulic fracturing stress measurements. In *Scale Effects in Rock Masses*, 289-295. AA Balkema Rotterdam.

Kendrick, D., M. Puskar, S. Schlotterbeck. 2005. Ultralightweight Proppants: A Field Study in the Big Sandy Field of Eastern Kentucky. SPE-98006-MS. Proc., SPE Eastern Regional Meeting.

King, G. E. 2010. Thirty years of gas shale fracturing: What have we learned? Proc., SPE Annual Technical Conference and Exhibition.

King, S. R. 1983. Liquid CO2 for the Stimulation of Low-Permeability Reservoirs. SPE-11616-MS.

Lecampion, B., J. Desroches, R. Jeffrey, A. Bunger. 2016. Experiments versus theory for the initiation and propagation of radial hydraulic fractures in low permeability materials. *Journal of Geophysical Research: Solid Earth*.

Lhomme, T., E. Detournay, R. Jeffrey. 2005. Effect of fluid compressibility and borehole radius on the propagation of a fluid-driven fracture. Proc., Proceedings of 11th International Conference on Fracture. Turin, Italy.

Li, X., L. Cui, J.-C. Roegiers. 1998. Thermoporoelastic modelling of wellbore stability in non-hydrostatic stress field. *International Journal of Rock Mechanics and Mining Sciences* **35** (4-5): 584.

Lillies, A. T., S. R. King. 1982. Sand Fracturing With Liquid Carbon Dioxide. Proc., SPE Production Technology Symposium, 8-9 November, Hobbs, New Mexico.

Mazza, R. L. 1997. Liquid CO2 improves Fracturing. *Hart's Oil and Gas World* **22**.

McDaniel, B., S. Grundmann, W. Kendrick, D. Wilson, S. Jordan. 1997. Field applications of cryogenic nitrogen as a hydraulic fracturing fluid. Proc., SPE Annual Technical Conference and Exhibition.

Nicot, J.-P., B. R. Scanlon. 2012. Water Use for Shale-Gas Production in Texas, U.S. *Environmental Science & Technology* **46** (6): 3580-3586.

Perkins, T., J. Gonzalez. 1985. The effect of thermoelastic stresses on injection well fracturing. *Society of Petroleum Engineers Journal* **25** (01): 78-88.

Rudenko, N. S., L. W. Schubnikow. 1968. The Viscosity of Liquid Nitrogen, Carbon Monoxide, Argon and Oxygen as a Function of Temperature, NASA–TT–F–11–868, 1–5.

Salimzadeh, S., A. Paluszny, R. Zimmerman. 2016. Thermal Effects during Hydraulic Fracturing in Low-Permeability Brittle Rocks. Proc., 50th US Rock Mechanics/Geomechanics Symposium.

Shaefer, M. T. 2005. Are Slick Water-Fracturing Applications Effective in the J-Sand Formation? Proc., SPE Annual Technical Conference and Exhibition, 9-12 October, Dallas, Texas.

Sharma, M. M., P. B. Gadde, R. Sullivan, R. Sigal, R. Fielder, D. Copeland, L. Griffin, L. Weijers. 2004. Slick Water and Hybrid Fracs in the Bossier: Some Lessons Learnt. Proc., SPE Annual Technical Conference and Exhibition, 26-29 September, Houston, Texas.

Sheahen, T. 1994. *Introduction to high-temperature superconductivity*, Springer Science & Business Media (Reprint).

Shimizu, H., S. Murata, T. Ishida. 2011. The distinct element analysis for hydraulic fracturing in hard rock considering fluid viscosity and particle size distribution. *International Journal of Rock Mechanics and Mining Sciences* **48** (5): 712-727.

Steward, D. B. 2013. George P. Mitchell And The Barnett Shale. *Journal of*

Petroleum Technology **65** (11): 58-68.

Tarasovs, S., A. Ghassemi. Propagation of a system of cracks under thermal stress. American Rock Mechanics Association.

Tarasovs, S., A. Ghassemi. 2014. Self-similarity and scaling of thermal shock fractures. *Physical Review E* **90** (1): 012403.

Wang, L., B. Yao, M. Cha, N. B. Alqahtani, T. W. Patterson, T. J. Kneafsey, J. L. Miskimins, X. Yin, Y.-S. Wu. 2016. Waterless fracturing technologies for unconventional reservoirs-opportunities for liquid nitrogen. *Journal of Natural Gas Science and Engineering* **35, Part A**: 160-174.

Wilson, D. R., R. M. Siebert, P. Lively. 1995. *Cryogenic coal bed gas well stimulation method*, Google Patents (Reprint). https://www.google.com/patents/US5464061.

Wu, B., X. Zhang, R. Jeffrey. 2010. A thermo-poro-elastic analysis of stress fields around a borehole. American Rock Mechanics Association.

Wu, B., X. Zhang, R. G. Jeffrey. 2016. Analysis of Thermal Effects on Hydraulic Fracturing Near a Horizontal Well by Using Displacement Discontinuity Method. SPE Asia Pacific Hydraulic Fracturing Conference.

Zhang, X., R. Jeffrey, B. Wu. 2014. Crack Propagation From a Surface Assisted by Fluid Pressure and Cooling. Proc., 48th US Rock Mechanics/Geomechanics Symposium.

Zhang, X., Y. Lu, J. Tang, Z. Zhou, Y. Liao. 2017. Experimental study on fracture initiation and propagation in shale using supercritical carbon dioxide fracturing. *Fuel* **190**: 370-378.

Zoback, M. D. 2010. *Reservoir geomechanics*, Cambridge University Press (Reprint).